Nanocomposite foams based on flexible biobased thermoplastic polyurethane and ZnO nanoparticles as potential wound dressing materials

NANOCOMPOSITE FOAMS BASED ON FLEXIBLE BIOBASED THERMOPLASTIC POLYURETHANE AND ZnO NANOPARTICLES AS POTENTIALWOUND DRESSING MATERIALS

Aleksandra Bužarovska[1], Sorina Dinescu[2], Andreea D. Lazar[2], Mirela Serban[2], Gratiela G. Pircalabioru[3], Marieta Costache[2], Chiara Gualandi[4], Luc Avérous[5]*

[1*]Faculty of Technology and Metallurgy, Sts Cyril and Methodius University, Rudjer Boskovic 16, 1000 Skopje, North Macedonia E-mail: abuzar@tmf.ukim.edu.mk

[2]Department of Biochemistry and Molecular Biology, University of Bucharest, Spl. Independentei 91-95, 050095 Bucharest, Romania

[3]Research Institute of University of Bucharest, University of Bucharest, Spl. Independentei 91-95, 050095 Bucharest, Romania

[4]Department of Chemistry "G. Ciamician" University of Bologna, Via Selmi2, 40126, and Advanced Mechanics and Materials – Interdepartmental Center, University of Bologna, Viale del Risorgimento 2, 40123 Bologna, Italy

[5]BioTeam/ICPEES-ECPM, UMR CNRS 7515, Université de Strasbourg, 67087 Strasbourg Cedex 2, France

Keywords

thermoplastic polyurethane, nanocomposite foams, wound dressings, biocompatibility, antibacterial activity

Abstract

In the present study biobased and soft thermoplastic polyurethane (TPU), obtained by polymerization from fatty acids, was used to produce TPU/ZnO nanocomposite foams by thermally induced phase separation method (TIPS). The produced foams were characterized and evaluated regarding their potential uses as wound dressing materials. The structure and morphology of the prepared flexible polymer foams with different content of ZnO nanofiller (1, 2, 5 and 10 wt% related to the polymer) were studied by

Fourier transform infrared spectroscopy (FTIR) and Scanning electron microscopy (SEM). Highly porous nanocomposite structure made of interconnected pores with dimensions between 10 and 60 μm was created allowing water vapor transmission rate (WVTR) up to 8.9 mg/cm^2·h. The TPU/ZnO foams, tested for their ability to support cells and their growth, showed highest cell proliferation for TPU nanocomposite foams with 2 and 5 wt% ZnO. Overall, the nanocomposite foams displayed a low cytotoxic potential (varied proportionally to the ZnO content) and good biocompatibility. All tested nanocomposite foams were found to be significantly active against biofilms formed by different Gram-positive (*Enterococcus faecalis* and *Staphylococcus aureus*) and Gram-negative (*Escherichia coli* and *Pseudomonas aeruginosa*) bacteria. Based on their behaviors, flexible TPU/ZnO nanocomposite foams can be considered for biomedical applications such as potential active wound dressing.

1. Introduction

Thermoplastic polyurethanes (TPUs) are synthetic polymers composed of phase-separated hard and soft segments. They are organized in microdomains due to phase segregation phenomena [1,2]. A variety of different aliphatic and aromatic TPUs can be produced from various types of polyols, mainly long polyesters or polyethers diols and short chain extenders, and diisocyanates. The properties of the PUs are primarily controlled by their chemical structures, morphologies and also by adjusting their hard segment (HS) contents. Therefore, a wide spectrum of different properties could be obtained with a controlled hydrophobicity-hydrophilicity balance from highly hydrophobic to highly hydrophilic character. TPU can be nowadays partially biobased

and obtained from renewable resources [3]. These biobased TPUs obtained from biomass present great advantages based on new macromolecular architectures [3].

During the last decades significant attempts have been made to find an appropriate use of PU for biomedical application. Most of the commercialized PUs are part of various implant devices such as pacemakers, heat valves, vascular prostheses and breast implants [4-6]. The reason for such a strong interest in PUs is due to the many advantages when using them as biomaterials; such as their macromolecular architecture diversities, good mechanical properties, as well as good biocompatibility with the surrounding tissues [7].

For instance, significant scientific attention has been given to finding appropriate applicability of PUs as wound dressing materials. Polyurethane based wound dressings were extensively studied for their high flexibility, low cytotoxicity, good water and controlled permeability as well as their wound healing capabilities [8,9]. However, some drawbacks still exist such as cytocompatibility, antimicrobial properties and hydrophilicity, thus providing space for further improvements of these materials.

In recent years, PU electrospun nanofiber mats have been developed as wound dressing materials [10-12]. The high specific area of these nanofiber mats was one of the conditions to produce promising wound dressing materials with excellent fluid handling capacity. PU membranes composing of various antibacterial polymers, natural components and nanofillers have been also widely investigated [13-15]. In particular, the addition of another polymer or nanofiller with antimicrobial properties to PU membranes was found to be effective in the wound healing process.

Diverse PU foams were developed as promising wound dressing materials with high capability for exudates absorption and adequate water vapor transmission rate [16, 17]. The lack of hydrophilicity or cell affinity toward these generally hydrophobic materials was overcome by their surface modifications [18, 19]. The use of different nanoparticles incorporated in the PU matrices could additionally change the structures thanks to interactions with the different polar groups in PU [20, 21].

In this work TPU/ZnO nanocomposite foams were produced by thermally induced phase separation method (TIPS) with the aim to combine the excellent mechanical properties of PUs with the interesting qualities of ZnO nanoparticles, including their antimicrobial properties [22,23] and their capability to promote cells adhesion and growth [24] for wound dressing applications. In the present study, the content of ZnO nanofiller was varied between 1 and 10 wt % related to the polymer, and the physico-chemical characteristics of the produced foams were observed by Fourier transform (FTIR) spectroscopy and Scanning electron microscopy (SEM). Furthermore, biocompatibility, cytotoxicity and antimicrobial activity were also studied.

2. Experimental section

2.1. Materials

The biobased polyester polyol used in this study was kindly supplied by Oleon (France). This polyol was based on dimeric fatty acids from rapeseed oil, with a purity higher than 98% and a mass-average molar mass (M_w) of 3300 $g.mol^{-1}$. Hydroxyl and acid values were 40 and 0.253 $mg.(g\ KOH)^{-1}$, respectively. 4,4-Diphenylmethane

diisocyanate (MDI) was supplied by Brenntag (France). 1,4-butanediol (BDO) was purchased from Sigma Aldrich (France).

ZnO nanoparticles (NM-110) was European Commission (JRC) sample. Dioxane (Merck) was used as solvent for foams preparation, while ethanol (Alkaloid product) was used for freeze extraction of dioxane. The solvents were used without further purification. Sample labeling and composition are given in Table 1.

2.2. Biobased TPU synthesis based on polyester polyol

TPU was prepared by polyaddition reaction between isocyanate groups (NCO) and hydroxyl groups (OH) by a two-step process. The final NCO/OH ratio was 1. HS content was 17 wt% in order to obtain a rather soft material at room temperature. The HS content was due to BDO and MDI content. During the first step, a prepolymer with NCO ending chains was obtained from polyaddition between the polyester polyol from dimer fatty acids and MDI. Then a short polyol, BDO, a chain extender is added to obtain high molar mass TPU.

In a first step, the polyol reacted with an excess of MDI (ratio 2:1) for 2 h in a five-necked round-bottom flask having the provision for nitrogen flushing, mechanical stirring and temperature control at 80 °C. At the end of this step the NCO consumption during this reaction was controlled. This result was used for the addition of the precise amount of diol in the processing step. In order to consider the high melt viscosity, the prepolymer was further melt-blended by “reactive processing” with the adequate amount of polyol and chain extender. The prepolymer synthesized in the first step and the calculated amount of polyol for a NCO/OH=1 ratio were directly introduced in the

feeding zone of an internal mixer (counter-rotating mixer Rheocord 9000, Haake, USA) equipped with a pair of high-shear roller-type rotors, at 80 °C, with a rotation speed of 50 rpm and 15 min processing time. Then, the adequate amount of BDO (chain extender) was added and the temperature was immediately increased to 180 °C for 8 min, without any catalyst. After polymerization, all systems were cured overnight in an oven at 70 °C to ensure the complete reaction of NCO groups. This multistep synthesis was previously described in another publication [25].

2.3. Preparation of TPU/ZnO foams

TPU was vacuum dried before dissolution in dioxane (5wt%) at 50°C for 24 hours. Appropriate content of ZnO nanofiller (1, 2, 5 and 10 wt% related to the polymer) was added to the stable TPU solution, mechanically stirred for 2 hours, and ultrasonically treated for 60 minutes. The prepared dispersions were poured into small petri dishes (d=5cm) and frozen at -30 °C. The samples were kept in deep freeze for 24 hours. The frozen polymer solution was immersed in a non-solvent bath to allow exchange of dioxane and ethanol at a temperature lower than the freezing point of the polymer solution [26, 27]. The freeze-extraction method provides extraction of the solvent using non-solvent before drying stage. The prepared foams were vacuum dried up to constant weight and further characterized.

2.4. Steric Exclusion Chromatography (SEC)

SEC measurements were performed with a Shimadzu instrument (Japan) equipped with a RID-10A refractive index detector. Chloroform was used as the mobile phase and the analyses were carried out at 25°C with a solvent flow rate of 0.8 mL. min^{-1}.

The columns used were PLGel Mixed-C and PLGel 100 A°. The calibration was performed with polystyrene standards from 580 to 1,650,000 $g.mol^{-1}$.

2.5. Microscopic analysis

Foams were fractured in liquid nitrogen and sections were observed by using a Leica Cambridge Stereoscan 360 Scanning Electron Microscope (SEM) operating at 20 kV. The samples were sputter-coated with gold prior to examination.

2.6. Thermal characterizations

TGA measurements were performed using Perkin Elmer, Pyris Diamond System in order to determine the nominal values of nanofiller content. The samples of around 5 mg weights were heated from 30 ^oC to 700 ^oC, with a heating rate of 10 °C min^{-1}, under constant nitrogen flow of 50 cm^3 min^{-1}.

Differential Scanning Calorimetry (DSC) measurements were carried out on a differential scanning calorimeter (Model Netzsch DSC 204 F1 Phoenix Instrument), in temperature regime starting from -80 to 160 ^oC, with a heating rate of 10 °C min^{-1}. The glass transition temperature was determined as midpoint on the thermal curve, corresponding to ½ of the heat flow difference between extrapolated onset and extrapolated end.

2.7. ATR-FTIR spectroscopy

FTIR spectroscopic analysis was performed using Perkin Elmer, Spectrum 100 FTIR spectrometer (USA). FTIR-ATR spectra were recorded with 32 scans in the range of 4000-600 cm^{-1}, with resolution of 4 cm^{-1}.

2.8. Contact angle measurements

The contact angle measurements were conducted under ambient temperature with a standard See System (Advex Instruments). A drop technique was applied, where 5-7 µl

of distilled water was deposited on a substrate and the contact angle was measured within 5 seconds. For each foam at least five drops were measured.

2.9. Water vapor transmission rate (WVTR)

The water vapor permeability of the investigated foams was measured gravimetrically using previously conditioned samples at 20 ^{o}C and relative humidity of 54%. Small glass tubes with diameter of 2 cm, filled with 5 ml of distilled water were covered and sealed well with sample foams and placed in desiccators with constant temperature and humidity. The weight changes were controlled in 30 minutes intervals within 24 h. The measurements were performed in duplicate. Water vapor transmission rate (WVTR) was determined as:

$$WVTR = (W_0 - W_t)t \cdot A$$

where W_o is the initial weight of the sealed tube and W_t is the weight of the tube at time t, while A is the area of the testing foam (cm^2).

2.10. Water uptake ability

Specimens with dimensions of 1cm x 1cm were immersed in 5 ml of phosphate buffer saline, PBS (pH=7.4). The samples were measured before and after the immersion for 4, 8, 24 and 48 hours at 37 ^{o}C. The water uptake was calculated as:

$$WU = (W_t - W_0) / W_0 \cdot 100$$

where W_0 is the weight of dry sample and W_t is the weight of the foam after relevant period of time t.

2.11. TPU/ZnO nanocomposite foams biocompatibility assessment

Human adipose-derived stem cells (hASC) were cultivated in direct contact with the TPU/ZnO nanocomposite foams. Cell suspension was distributed over the scaffolds,

allowed to adhere for 24h, and the resulting cell-scaffold constructs were maintained in standard culture conditions (37 ^{o}C, 5% CO_2 and humidity) for up to 7 days. For biocompatibility studies, a bidimensional tissue culture plastic control (TCPS) was considered. In addition, to assess the effect of ZnO nanofiller on the biocompatibility, a neat TPU material was considered as a second reference (TPU). MTT assay was used for evaluation of cell viability and proliferation potential, after 2 and 7 days of culture. Cell-scaffold constructs were incubated with 1 mg/mL MTT solution for 4 h at 37^{o}C. The resulted formazan crystals were solubilized with isopropanol and optic density of the solution was measured at 550 nm on Flex Station 3 spectrophotometer (Molecular Devices, USA). Cytotoxic potential of TPU/ZnO nanocomposite scaffolds was tested with LDH assay, versus TCPS and TPU controls. The culture media was collected from the bioconstructs, mixed with the components of the Tox7-KT kit (Sigma, Steinheim, Germany), according to manufacturer's instructions, and the resulting solution was measured by spectrophotometry at 490 nm. A qualitative method, namely Live/Dead assay, was used to determine the ratio between live cells (green) and dead cells (red). The cell-scaffold constructs were incubated for 30 min with the mixed solution containing calcein-AM and ethidium bromide homodimer (EthD-1) fluorescent dyes. Images were obtained in confocal microscopy using Zeiss LSM 710 system and corresponding ZEN software. All tests were performed in triplicate. Statistical analysis of the data was performed with GraphPad Prism software, one-way ANOVA method, taking as statistically significant a p value < 0.05.

2.12. TPU/ZnO antimicrobial activity

The antimicrobial activity harbored by the novel biomaterials containing ZnO was evaluated against Gram-positive and Gram-negative bacteria. Gram-positive *Enterococcus faecalis* ATCC 29212, *Staphylococcus aureus* ATCC 25923 and Gram-negative *Escherichia coli* A TCC 8739, and *Pseudomonas aeruginosa* ATCC 27853 bacterial strains were purchased from (ATCC, USA). Glycerol stocks were streaked on Mueller Hinton agar to obtain 24 h cultures to be used for all further studies. Monospecific biofilm development was assessed at 4 h after exposure. The materials were cut in equal circular pieces of 6 mm and sterilized by UV exposure for 20 min. These were further immersed in 1 mL of microbial suspensions of ~10^7 colony forming units (CFU)/mL and were left in contact for 4 h. At the end of this time interval, microbial suspensions incubated with the tested samples were vortexed, serially ten-fold diluted, and 10 µL of each serial dilution was plated in triplicate on LB agar. After 24 h of incubation at 37 °C, viable cell counts were performed in order to obtain CFU/mL for each sample. Data shown as Mean+SEM, n=3, ***$p<0.001$, **$p<0.01$, *$p<0.05$ by Unpaired t- test.

3. Results and discussion

3.1. Molecular characteristics

Molar mass and dispersity of the biobased TPU have been determined by SEC. The mass-average molar mass is rather consistent for a biobased TPU (M_w=160 Kg.mol^{-1}) with a rather high dispersity (Đ=6.2).

3.2. Morphological characterization

TPU/ZnO foams produced by TIPS appeared as flexible membranes with a thickness ranging from 150 to 230 µm. Information on 3D microstructure, pore

dimensions and on the quality of ZnO dispersion were obtained by SEM inspection (Figure 1). Low-magnification images show that all foams have a similar highly porous structure made by irregular and frequently interconnected pores with dimension in the range 10-60 μm. Such a structure is expected to be morphologically suitable to maintain a proper environment at the wound/dressing interface by absorbing excess exudates, allowing gaseous and fluid exchanges. High-magnifications of TPU-2, TPU-5 and TPU-10 revealed the presence of well-dispersed and well-separated ZnO nanoparticles, whose dimension ranges from 50 to 250 nm (in line with supplier specifications) [28]. As expected, the amount of nanoparticles detectable on the surface of pore walls increased with the increase of the ZnO loading, thus supporting the nominal amount of ZnO added during foam preparation.

3.3. Thermal and structural characterization

Thermogravimetric measurements were performed in order to precisely quantify the amount of the added nanofiller and to analyze the thermal behavior of the prepared foams. The TGA graphs are presented in Figure 2, and all relevant data as temperature onsets and weight residues at 600 °C are collected in Table 2. The amount of incorporated ZnO was determined by taking into account that the weight residue of the composite is a sum of weight residuals of neat TPU and ZnO multiplied by their weight fractions i.e. $W_{res,c} = W_{ree,TPU} \times wt_{TPU} + W_{res,ZnO} \times wt_{ZnO}$, assuming that $wt_{TPU} + wt_{ZnO} = 1$. In the above equations, $W_{res,c}$, $W_{res,TPU}$ and $W_{res,ZnO}$ are the weight residuals of the composite, TPU and ZnO respectively, while wt_{TPU} and wt_{ZnO} are the weight fractions of TPU and ZnO in the coresponding composite. The weight residues at 600 °C confirmed the values of added nanofiller in the related foams.

The thermal degradation of TPU and its composite foams proceeded as a two-step degradation process. The onset temperature of the first degradation step TPU shifted to lower temperatures with the increasing of nanofiller content, while the temperature onset of the second degradation process slight increased compared to pure TPU. The initial decomposition process is usually connected to the degradation of hard segments in polyurethanes, while the decomposition of the soft segment is arising at higher temperatures (second decomposition process) [29]. The increased content of nanofiller generally promotes the degradation of the pure polymer matrix as it was previously observed [30]. In this case, the decrease of the first decomposition temperature might be additionally attributed to inhibition of the possible hydrogen bonds between ZnO nanoparticles and TPU matrix [31].

DSC thermograms (Figure 3) of neat TPU and its nanocomposite foams, obtained in the temperature region between -80 and 160 ^{o}C, clearly show two distinct glass transition temperatures T_g; one in the lower temperature region (around -46 ^{o}C) and one in the higher temperature region, with no visible melting endotherms, suggesting on completely amorphous polymer foams [25]. As TPU is based on soft and hard segments, the T_g in the lower temperature region corresponds to soft segment, while the T_g in the upper temperature region is correlated to the HS in TPU [3]. The values obtained from the first scan of the measurements are collected in Table 2. It could be seen that the $T_g s$ in the lower temperature region are pretty independent of the nanofiller content, while the $T_g s$ at the upper temperature region were found to be significantly influenced by the nanofiller content. The second T_g is linked to the rigid urethane bonds and their vicinities. These T_gs were moved to higher temperatures, thus suggesting a local decreased mobility of the

macromolecular chains due to possible interactions between the nanofiller and the TPU matrix, mainly at the level of the polar urethane bonds. It could be also noticed that this increase of T_g with the nanoparticles loadings has irregular trend. These discrepancies could be additionally attributed to the complex interactions between the ZnO nanoparticles and the polymer matrix. Namely, surface -OH groups in some sense could compete with the -NH groups when they are interacting with carbonyl groups of the urethane bonds, changing the nanocomposite properties [32, 33]. The T_g could be additionally affected by nanoparticles distribution as well as their size. Taking into account that SEM images have shown well-dispersed ZnO nanoparticles, this behavior of irregular changes in T_g could be additionally attributed to different sizes of the nano fillller particles (ranged from 50 to 250 nm) rather than their distribution [34].

FTIR spectroscopy measurements were performed in order to detect and verify the possible interactions between the nanofiller and the polymer matrix. All FTIR-ATR spectra of TPU and its nanocomposite foams, in the range between 4000 and 600 cm^{-1} are presented in Figure 4. The broad absorption band at 3333 cm^{-1} is indicative of partially hydrogen bonded N-H stretch in the urethane group, while the small shoulder at 3450 cm^{-1} is due to non-hydrogen bonded urethane N-H stretch (Figure 4A) [35,36]. The strong absorptions positioned at 2922 cm^{-1} and 2852 cm^{-1} are associated with the CH_2 asymmetric and symmetric stretch vibrations. The characteristic peak at 1734 cm^{-1}, accompanied with strong shoulder absorption at 1706 cm^{-1} is indicative of non-hydrogen bonded and hydrogen bonded carbonyl stretch of the urethane group, respectively. To evaluate if the -OH groups on ZnO nanoparticles surface have an influence on the

formation of hydrogen bond in the presence of urethane group, as previously found [37] the hydrogen bonded index (HBI) was determined as:

$$HBI=A_{C=O\ bonded}/A_{C=O\ free}$$

where $A_{C=O\ bonded}$ and $A_{C=O\ free}$ correspond to the integrated areas of absorption bands positioned at 1706 cm^{-1} and 1734 cm^{-1} respectively [38, 39]. Since these two bands related to the bonded and free carbonyls were not well separated, curve fitting simulations were performed using Origin 8.1 software. The bands were deconvoluted by considering peaks as Gaussian (Figure 4B). The estimated HBI according to the above-mentioned expression are collected in Table 3 and ranged between 1.03 to 1.36, indicating that the existence of nanofiller free -OH groups participate in the formation of hydrogen bonding with urethane carbonyl groups. It could be also observed that HBI increased with the increasing of nanofiller content, but at higher contents of ZnO nanoparticles (TPU-10), the HBI had lower value. This phenomenon could be explained by the possible agglomeration of the filler that decreases its participation in the formation of hydrogen bond between -OH surface groups and the urethane group.

The contact angle measurements give a clear picture for the hydrophilic/hydrophobic character of the materials. They are usually performed on ideally flat surfaces but in case of polymer foams these measurements could confer qualitatively assessment of the hydrophilic character of the materials. The results given in Figure 5 are actually average values (n=5) indicating increased values of the contact angles with the increased content of nanofiller, from 116.7 ± 0.9^{o} (TPU) up to 126.6 ± 1.4^{o} (TPU-10), confirming the increased hydrophobicity of the foams. Surprisingly, increased contact angles of the foams with higher content of ZnO nanofiller considering

its hydrophilic character, could additionally validate the possible interactions of ZnO surface -OH groups and urethane group of TPU (previously confirmed by DSC and FTIR analyses). Similar behavior was detected in PU blend films, where ZnO nanofiller was found to diminish the hydrophilic character of the composites [40]. The hydrophilic character of the materials is desired attribute in many biological applications, but on the other side hydrophobicity could be a positive aspect when using these materials for example as blood vessels [41].

3.4. Water vapor permeability and water uptake ability of TPU/ZnO foams

The WVTR is an important parameter when testing certain biomaterials as wound dressings. An ideal wound dressing should possess certain permeability that allows the open wounds optimal moisture and free drainage [42]. Commercial wound dressings have WVTR between 8.3 and 10.5 mg/cm^2 ·h [43]. The results obtained from the investigated foams within 24 hours were determined in the range between 8.0±0.06 and 8.9±0.09 mg/cm^2·h (Table 4), thus representing relevant and promising results for wound dressing application of these materials.

The water absorptivity of a certain material is mainly governed by the hydrophilic character of the material that might arise from the polymer matrix as well as the nanofiller, since most of the nanoparticles have certain hydrophilicity due to the existence of surface -OH groups. The water uptake behavior performed within 48 hours confirmed (Figure 6) limited water-uptake due to the hydrophobic character of the prepared polymer foams. The water-uptakes in nanocomposite foams were even lower, since the ZnO filler was confirmed to participate in the formation of hydrogen bonding; therefore its

hydrophilic character was diminished as previously confirmed. Higher water uptake is usually connected to higher WVPR.

The low water uptakes and relatively high WVPR in our case could be due to a complex mechanism influenced by two processes: water solubility in the surface layers of the polymer foam, and diffusivity of the water molecules within the polymer foam [44]. The first process is generally dependent on the free volume of the polymer matrix and availability of polar groups (arising from the polymer matrix and nanofiller). The diffusion process is governed by free movement of water molecules and "trapped" water molecules due to hydrogen bonding. Therefore, the water diffusion process could be highly dependent on these "traps" as well as strength of hydrogen bonds; in our systems, water-polymer and water-nanofiller. According to this complex mechanism, the water uptakes could not be in a straightforward correlation with WVPR.

Wound dressing materials should possess higher water-uptake ability in order to accumulate the excess fluid from the wound. This limitation in water-uptake in our systems is actually compensated by the relatively good WVTR determined in all samples that was primarily governed by the porosity structure, and thickness of the materials rather than their hydrophilicity.

3.5. Viability and proliferation potential of hASC in contact with TPU/ZnO nanocomposites

TPU and TPU-based scaffolds filled with different content of ZnO were comparatively tested for their ability to support the cells growth and development. The viability of hASC in contact with the nanocomposites was quantitatively evaluated by MTT assay after 2 and 7 days of culture in standard conditions (Figure 7), by comparison with a standard TCPS control and the neat TPU foam. After 2 days, the results showed a

significant difference ($p<0.05$) between TPU/ZnO scaffolds and the neat TPU control sample in regards to cell viability. In particular, higher levels of cell viability were detected for the composites with a higher percentage of ZnO (TPU-2, TPU-5 and TPU-10), compared to the TPU control ($p<0.05$). A similar level of cell viability was detected on all cell-scaffold constructs one week after seeding, comparable to the one found in TCPS. Significant positive differences were reported between the TPU control and TPU-2 and TPU-5 nanocomposite foams ($p<0.05$), showing possible improvement of cell response when adding 2 or 5% ZnO nanoparticles. Instead, no meaningful difference was found in the presence of 10% ZnO nanofiller as compared to pure TPU, but rather a decrease in cell viability when compared to TCPS control ($p<0.05$). This may suggest that the addition of ZnO nanofiller in the TPU matrix has a positive impact on cell behavior and growth, but the addition of nanoparticles in excess (10%) appears to inhibit cell viability.

Between 2 and 7 days of culture, significant proliferation was registered for TPU-1, TPU-5 scaffolds ($p<0.001$) and, to a lesser extent, for TPU-10 ($p<0.05$). Highest proliferation rates were reported for TPU-2 and TPU-5 confirming our hypothesis. In conclusion, in regards to viability and proliferation potential of hASC, the most biocompatible nanocomposites appear to be TPU-2 and TPU-5.

3.6. Cytotoxic potential of TPU/ZnO nanocomposites

The cytotoxic potential of the TPU-based nanocomposites was indicated by the proportion of dead cells shown by the levels of LDH released in the culture media (Figure 8). After 2 days of culture, similar levels of cytotoxicity were reported for TPU/ZnO scaffolds in comparison to TPU and TCPS controls, except for a considerable

increase in cytotoxicity displayed on TPU-10 ($p<0.05$) and a slight decrease in TPU-1 and TPU-5. The same difference ($p<0.05$) was detected between TPU-10 and the TPU control sample after one week of culture ($p<0.01$ when compared to TCPS control), supporting the data previously obtained with MTT assay. Overall, TPU/ZnO nanocomposites display a low cytotoxic potential, which possibly varies proportionally to the ZnO concentration.

3.7. Qualitative analysis of live and dead cells in TPU/ZnO

Fluorescent staining (Live/Dead assay) and confocal microscopy allowed the qualitative analysis of live (green) and dead (red) cells, as well as the observation of cell morphology and distribution in contact with TPU-based nanocomposites (Figure 9).

After 2 days of culture, a considerate amount of living (green) cells were detected on all scaffolds, independent of ZnO concentration, particular in TPU-2. After 7 days of culture, a higher number of living cells (green) were observed on the TPU/ZnO composites, in comparison to the pure TPU control sample, suggesting that the addition of ZnO nanofiller to a certain proportion promoted biocompatibility properties for TPU/ZnO nanocomposites. In addition, the images also revealed the possibility of cells to group, particularly on TPU with 2% and 5% ZnO nanoparticles.

All scaffolds displayed good biocompatibility, with a much higher proportion of living (green) cells than dead (red) cells. However, on TPU-10 foam, cells lost their fibroblast-like shape, became more round and formed tighter groups. This is consistent with the results of quantitative MTT and LDH assays.

3.8. Antimicrobial activity

The novel materials containing different ZnO concentrations obtained and characterized within this study revealed antimicrobial activity. For all tested strains, ZnO addition lead to a significant decrease in bacterial viability. For Gram-positive bacteria (*S. aureus* and *E. fecalis*), the highest ZnO concentration (TPU-10) led to a 10^3 CFU reduction (Figure 10 A, B). Similarly, in case of Gram-negative bacteria (P. aeruginosa, E.coli), TPU-10 significantly decreased viability (Figure 10 C, D), namely the highest ZnO concentration (10%) led to a 10^3 fold reduction in CFUs compared to simple TPU. Our results in terms of antibacterial activity of TPU/ZnO composites are in accordance with other studies. ZnO nanoparticles were reported to be active against biofilms formed by different bacterial and fungal species [45, 46]. Seil and Webster incorporated ZnO nanoparticles (60 nm diameter) into PVC. In order to quantify the antimicrobial activity of ZnO-NPs against *S. aureus* (ATCC 25923) biofilms, the authors treated a PVC membrane with different concentrations of ZnO-NPs (0%, 2%, 10%, 25%, and 50%, w/v) and further inoculated 3×10^6 CFU *S. aureus* (ATCC 25923). The polymer composites with ZnO-NPs exhibited a reduction in the number of total bacterial count as compared to those without ZnO-NPs (control). Crystal violet staining analysis showed a 55% reduction in biofilm formation on the surface of the composites containing different concentrations of ZnO-NPs compared to the control however the difference in the reduction in biofilm formation at the different concentrations of polymer ZnO-NPs composites was not significant [46]. Lee *et al.* analyzed the anti-biofilm activity of Zn^{2+} and/or ZnO-NPs against *P. aeruginosa* PAO1, *E. coli* O157:H7 (ATCC 43895), methicillin-sensitive *S. aureus* (MSSA; ATCC 6538) and a methicillin-resistant *S. aureus*

(MRSA; ATCC BA-1707). ZnO (5 mM) was able to inhibit biofilm formation of *E. coli* O157:H7, MSSA (ATCC 6538), and MRSA (ATCC BA-1707). In case of *P. aeruginosa,* biofilm formation on polystyrene surfaces was inhibited by $ZnCl_2$ and $Zn(NO_3)_2$ in a dose-dependent manner, whereas ZnO (1 mM; average diameter 50 nm) reduced biofilm formation by 95% [45].

Micro-sized ZnO spheres exhibited high anti-biofilm activity against Gram-positive (*S. aureus, B. subtilis*) and Gram-negative (*E. coli, K. pneumoniae, P. aeruginosa*) reference and resistant clinical strains, demonstrating a promising potential for the development of new ZnO anti-biofilm formulations [47].

ZnO-NPs with an average size of 20 nm obtained by Sangani *et al.* using a sol–gel procedure inhibited biofilm formation by 15 clinical isolates and one reference (ATCC 9027) strain of *P. aeruginosa* at a concentration of 350 μg/mL [48]. ZnO-NPs with a size in the range of 10–15 nm inhibited *P. aeruginosa* biofilm formation at 50 and 100 μg/mL concentrations [49]. The interplay between ZnO-NPs and the bacterial inoculum releases reactive oxygen species (ROS) involved in biofilm inhibition. High ROS production was correlated to the increase in antibacterial activity of ZnO-NPs; hence, the mechanism of action may be due to the higher ROS production.

4. Conclusion

Biobased TPU/ZnO nanocomposite foams have been successfully elaborated and characterized for potential wound dressing materials. The nanofiller-TPU interactions have been clearly shown and localized in the nanocomposite-based foams.

Highly porous foams were created with structure made of interconnected pores with dimensions between 10 and 60 μm. The FTIR spectroscopy revealed formation of

hydrogen bonding between surface hydroxyl groups of ZnO nanoparticles and polar urethane group, thus affecting the glass transition temperature of the HS, as well as lower absorptivity of the investigated foams when compared to the neat TPU. The highly porous structure was responsible for acceptable WVTR of up to 8.9 mg/cm^{2}·h.

The incorporation of ZnO up to 5wt% loadings has a positive impact on cell behavior and growth, while at its higher content (10 wt%), the addition of nanoparticles appeared to inhibit cell viability. Overall, the TPU/ZnO nanocomposite foams displayed low cytotoxic potential and were found to be very effective against Gram-positive and Gram-negative bacteria.

Acknowledgement

This work was partially supported by the project Composite Materials Based on Biopolymers and Ceramic Particles, with Applications in Tissue Engineering and Controlled Drugs Delivery (BIOCOMPMAT), developed in cooperation with the University Agency for Francophony (AUF). Biocompatibility and antimicrobial activity studies were supported by a grant of the Romanian Ministry of Research and Innovation, CCCDI-UEFISCDI, project number PN-III-P1-1.2-PCCDI-2017-0782/REGMED Project3, within PNCDI III.

References

[1] The polyurethanes book, ed. D. Randall and S. Lee, Huntsman Polyurethanes, New York, Distributed by John Wiley & Sons, Everberg, Belgium, **2002**

[2] E. Hablot, D. Zheng, M. Bouquey, L. Avérous, Polyurethanes based on castor oil: kinetics, chemical, mechanical and thermal properties, Macromol. Mater. Eng. 293 (2008) 922-929.

[3] M. Reulier, L. Avérous, Elaboration, morphology and properties of renewable thermoplastic blends, based on polyamide and polyurethane synthesized from dimer fatty acids, Eur. Polym. J. 67 (2015) 418-427.

[4] SQ. Liu, M. Kodama, Porous polyurethane vascular prostheses with variable compliances, J. Biomed. Mater. Res. 26 (1992) 1489-1502.

[5] D. Hoffman, D. Sisto, LS. Yu et al, Evaluation of stended polyurethane mitral valve prosthesis, Trans Am. Soc. Artif. Intern. Organs 37 (1991) M354-355.

[6] A. Capozzi, VR. Pennisi, Clinical experience with polyurethane-covered gel-filled mammary prostheses, Plast. Reconstr. Surg, 68 (1981) 512-518.

[7] P. Vermette, H.J. Griesser, G. Laroche, R. Guidoin, Biomedical Application of Polyurethanes. Eurekah.com Georgetown, Texas USA **2001**

[8] M. Sahraro, H. Yeganeh, M. Sorayya, Guanidine hydrochloride embedded polyurethanes as antimicrobial and absorptive wound dressing membranes with promising cytocompatibility, Mater. Sci. Eng. C 59 (2016) 1025-1037.

[9] X. Liu, Y. Niu, K.C. Chen, S. Chen, Rapid hemostatic and mild polyurethane-urea foam wound dressing for promoting wound healing, Mater. Sci. Eng. C 71 (2017) 289-297.

[10] H. Shi, H. Liu, S. Luan, D. Shi, S.Yan, C. Liu, Antibacterial and biocompatible properties of polyurethane nanofiber composites with integrated antifouling and bactericidal properties, Compos. Sci. Technol. 127 (2016) 28-35.

[11] A.R. Unnithan, G. Gnanasekaran, Y. Sathishkumar, Y.S. Lee, C.S. Kim, Electrospun antibacterial polyurethane-celulose acetate-zein composite mats for wound dressing, Carbohydr. Polym. 102 (2014**)** 884-892.

[12] Y.Wang, P. Li, P.Xiang, J. Lu, J. Jyuan, J. Shen, Electrospun polyurethane/keratin/AgNP biocomposite mats for biocompatible antibacterial wound dressings, J. Mater. Chem. 4 (2016) 635-648.

[13] S.J. Lee, D.N. Heo, J-H. Moon, H.N. Park, W-K. Ko, M.S. Bae, J.B. Lee, S.W. Park, E-C. Kim, C.H. Lee, B-Y. Jung, I.K. Kwon, Chitosan/Polyurethane Blended Fiber Sheets Containing Silver Sulfadiazine for Use as an Antimicrobial Wound Dressing, J. Nanosci. Nanotechnol. 14 (2014) 7488-7494.

[14] J.I. Kim, H.R. Pant, H-J. Sim, K.M. Lee, C.S. Kim, Electrospun propolis/polyurethane composite nanofibers for biomedical applications, Mater. Sci. Eng. C 44 (2014) 52-57.

[15] J-P. Chen, Y. Chiang, Bioactive Electrospun Silver Nanoparticles-Containing Polyurethane Nanofibers as Wound Dressing, J. Nanosci. Nanotechnol. 10 (2010) 7560-7564.

[16] E-H. Song, S-H. Jeong, J-U. Park, S. Kim, H-E. Kim, J. Song, Polyurethane-silica hybrid foams from a one-step foaming reaction, coupled with a sol-gel process for enhanced wound healing, Mater. Sci. Eng. C 79 (2017) 866-874.

[17] D.G. Pyuna, H.J. Choia, H.S. Yoonb, T. Thambic, D.S. Leec, Polyurethane foam containing rhEGF as a dressing material for healing diabetic wounds: Synthesis, characterization, in vitro and in vivo studies, Colloids. Surf. B Biointerfaces 135 (2015) 699-706.

[18] C. Luo, W. Liu, B. Luo, J. Tiana, W. Wen, M. Liu, C. Zhou, Antibacterial activity and cytocompatibility of chitooligosaccharide-modified polyurethane membrane via polydopamine adhesive layer, Carbohydr. Polym. 156 (2017) 235-243.

[19] A. Rezapour-Lactoee, H. Yeganeh, S.N. Ostad, R. Gharibi, Z. Mazaheri, J. Ai, Thermoresponsive polyurethane/siloxane membrane for wound dressing and cell sheet transplantation: In-vitro and in-vivo studies, Mater. Sci. Eng. C 69 (2016) 804-814.

[20] L. Yan, S. Si, Y. Chen, T. Yuan, H. Fan, Y. Yao, Q. Zhang, Electrospun In-situ Hybrid polyurethane/Nano-TiO_2 as wound dressings, Fiber. Polym. 12 (2011) 207-213.

[21] M. Shahrousvand, M.S. Hoseinian, M. Ghollasi, A. Karbalaeimahdi, A. Salimi, F.A. Tabar, Flexible magnetic polyurethane/Fe_2O_3 nanoparticles as organic-inorganic nanocomposites for biomedical applications: Properties and cell behavior, Mater. Sci. Eng. C 74 (2017) 556-567.

[22] M. Laurenti, V. Cauda, ZnO Nanostructures for Tissue Engineering Applications, Nanomaterials 7 (2017) 374.

[23] L. Grenho, C.L. Salgado, M.H. Fernandes, F.J. Monteiro, M.P. Ferraz, Antibacterial activity and biocompatibility of three-dimensional nanostructured porous granules of hydroxyapatite and zinc oxide nanoparticles- an in vitro and in vivo study, Nanotechnology 26 (2015) 315101.

[24] Y. Zhang, TR. Nayak, H. Hong, W. Cai, Biomedical application of zinc oxide nanomaterials, Curr. Mol. Med. 13 (2013) 1633-1645.

[25] C. Bueno-Ferrer, E. Hablot, F.P. Sarazin, M.C. Garrigo´s, A. Jime´nez, L. Averous, Structure and Morphology of New Bio-Based Thermoplastic Polyurethanes Obtained from Dimeric Fatty Acids, Macromol. Mater. Eng. 297 **(**2012) 777-784.

[26] 26. M-H Hoa, P-Y Kuoa, H-J Hsieha, T-Y Hsienb, L-T Houc, J-Y Laid, D-M Wanga, Preparation of porous scaffolds by using freeze-extraction and freeze-gelation methods, Biomaterials 25 (2004) 129–138.

[27] A. Buzarovska, C. Gualandi, A. Parrilli, M. Scandola, Effect of TiO_2 nanoparticle loading on Poly(L-lactic acid) porous scaffolds fabricated by TIPS, Compos. Part B Eng. 81 **(**2015) 189-195.

[28] European Commission, Joint Research Centre, Institute for Reference Materials and Measurements, JRC 64075, NM-Series of Representative Manufactured Nanomaterials, Luxembourg: Publications Office of the European Union **2011**

[29] D. Wang, G. Zhang, Y. Zhang, Y. Gao, Y. Zhao, C. Zhou, et al., Synthesis, characterization and properties of novel polyether ester polyols and developed polyurethanes, J. Appl. Polym. Sci. 103 (2007) 417-424.

[30] A. Buzarovska, Preparation and characterization of poly(ε-caprolactone)/ZnO foams for tissue engineering applications, J. Mater. Sci. 52 (2017) 12067-12078.

[31] A. Mohammadi, M. Barikani, M. Barmar, Synthesis and investigation of thermal and mechanical properties of in situ biocompatible Fe_3O_4/polyurethane elastomer nanocomposites, Polym. Bull. 72 (2015) 219-234.

[32] J. Zheng, R. Ozisik, RW Siegel, Disruption of self-assembly and altered mechanical behavior in polyurethane/zinc oxides nanocomposites. Polymer 46 (2005) 10873–10882.

[33] G. Polizos, E. Tuncer, AL. Agapov, D. Stevens, AP. Sokolov, MK Kidder, JD. Jacobs, H. Koerner, RA. Vaia, KL. More, I. Sauers, Effect of polymer–nanoparticle interactions on the glass transition dynamics and the conductivity mechanism in polyurethane titanium dioxide nanocomposites, Polymer 53 (2012) 595–603.

[34] O.A. Serenko, V. I. Roldughin, A. A. Askadskii, E. S. Serkova, P.V. Strashnov, Z. B. Shifrina, The effect of size and concentration of nanoparticles on the glass transition temperature of polymer nanocomposites, RSC Adv. 7 (2017) 50113-50120.

[35] I. Yilgor, E. Yilgor, I.G. Guler, T.C. Ward, G.L. Wilkes, FTIR investigation of the influence of diisocyanate symmetry on the morphology development in model segmented polyurethanes, Polymer 47 (2006) 4105-4114.

[36] T.S. Velayutham, W.H. Abd Majid, W.C. Gan, A. Khorsand Zak, S.N. Gan, Theoretical and experimental approach on dielectric properties of ZnO nanoparticles and polyurethane/ZnO nanocomposites, J. Appl. Phys. 112 (2012) 054106.

[37] B. Molki, W.M. Aframehr, R. Bagheri, J. Salimi. Mixed matrix membranes of polyurethane with nickel oxide nanoparticles for CO_2 gas separation, J. Membrane. Sci. 549 (2018) 588-601.

[38] R. Seymour, G. Estes, S.L. Cooper, Infrared studies of segmented polyurethane elastomers. I. Hydrogen bonding, Macromolecules 3 (1970) 579-583.

[39] C.L. Zhang, J. Hu, S.J. Chen, Theoretical Study of Hydrogen Bonding Interactions on MDI-Based Polyurethane, J. Mol. Model. 16 (2010) 1391-1399.

[40] K. Marycz, M. Maredziak, J. Grzesiak, D. Szarek, A. Lis, J. Laska, Polyurethane/Polylactide-Blend Films Doped with Zinc Ions for the Growth and Expansion of Human Olfactory Ensheathing Cells (OECs) and Adipose-Derived Mesenchymal Stromal Stem Cells (ASCs) for Regenerative Medicine Applications, Polymers 8 (2016) 175.

[41] T-H. Nguyen, A.R. Padalhin , H.S. Seo, B-T. Lee, A hybrid electrospun PU/PCL scaffold satisfied the requirements of blood vessel prosthesis in terms of mechanical properties, pore size, and biocompatibility, J. Biomater. Sci. Polym. Ed 24 (2013) 1692-1706.

[42] J.G. Lundin, C.L. McGann, G.C. Daniels, B.C. Streifel, J.H. Wynne, Hemostatic kaolin-polyurethane foam composites for multifunctional wound dressing applications, Mater. Sci. Eng. C 79 (2017) 702-709.

[43] LR. Cardona, YD. Sanzgiri, LM. Benedetti, VJ. Stella, EM Topp, Application of benzyl hyaluronate membranes as potential wound dressing: evaluation of water vapor and gas permeabilities, Biomaterials 17 (1996) 1639-1643.

[44] P. Gilormini, J.Verdu, On the role of hydrogen bonding on water absorption in polymers, Polymer 142 (2018) 164-169.

[45] JH. Lee, YG. Kim, MH. Cho J. Lee, ZnO nanoparticles inhibit Pseudomonas aeruginosa biofilm formation and virulence factor production, Microbiol. Res. 169 (2014) 888-896.

[46] JT. Seil. TJ. Webster, Reduced Staphylococcus aureus proliferation and biofilm formation on zinc oxide nanoparticle PVC composite surfaces, Acta Biomater. 7 (2011) 2579-2584.

[47] G. Patrinoiu, JM. Calderón-Moreno, CM. Chifiriuc, C. Saviuc, R. Birjega, R.O. Carp, Tunable ZnO spheres with high anti-biofilm and antibacterial activity via a simple green hydrothermal route, J. Colloid. Interface. Sci. 15 (2016) 64-74.

[48] MH. Sangani, MN. Moghaddam MM. Forghanifard, Inhibitory effect of zinc oxide nanoparticles on pseudomonas aeruginosa biofilm formation, Nanomedicine J. 2 (2015) 121-128.

[49] S. Dwivedi, R. Wahab, F. Khan, YK. Mishra, J. Musarrat AA. Al-Khedhairy, Reactive oxygen species mediated bacterial biofilm inhibition via zinc oxide nanoparticles and their statistical determination, PLoS One 9 (2014) e111289.

Figure legends

Figure 1. SEM images of TPU foams loaded with different amounts of ZnO nanoparticles: TPU (A, B); TPU-1 (C, D); TPU-2 (E, F, G); TPU-5 (H, I, J); TPU-10 (K, L, M). Scale bars: 10 µm (A, C, E, H, K); 2 µm (B, D, F, I, L); 1 µm (G, J, M).

Figure 2. TGA graphs of TPU nanocomposite foams: neat TPU (a); TPU-1 (b); TPU-2 (c); TPU-5(d); TPU-10 (e).

Figure 3. DSC plots of TPU and TPU/ZnO nanocomposite foams. First heating runs.

Figure 4. FTIR spectra of TPU and TPU/ZnO nanocomposite foams. (A) Region between 3600 and 3200 cm^{-1}, (B) Deconvolutied peaks positioned at 1734 and 1706 cm^{-1}.

Figure 5. Water contact angles of TPU and its nanocomposite foams

Figure 6. Water uptake of neat TPU and TPU/ZnO nanocomposite foams over a period of time

Figure 7. Viability and proliferation of hASCs seeded on TPU/ZnO materials measured by MTT assay, after 2 and 7 days of culture in standard conditions. Statistical significance: * $p<0.05$ (comparison between different samples during one time point); # $p<0.05$; ### $p<0.001$ (comparison of the same sample between different time points).

Figure 8. Cytotoxicity of TPU/ZnO materials revealed by LDH assay over 7 days of standard culture. Statistical significance: * $p<0.05$; ** $p<0.01$.

Figure 9. Live (green) and dead (red) cells detected on TPU/ZnO materials with fluorescent staining (Live/Dead assay) and confocal microscopy.

Figure 10. Evaluation of the antimicrobial activity against Gram positive (A, B) and Gram negative (C, D) bacteria

Supplementary materials

SM1. FTIR spectrum of ZnO nanoparticles
SM2. Viability and cytotoxicity in percentages

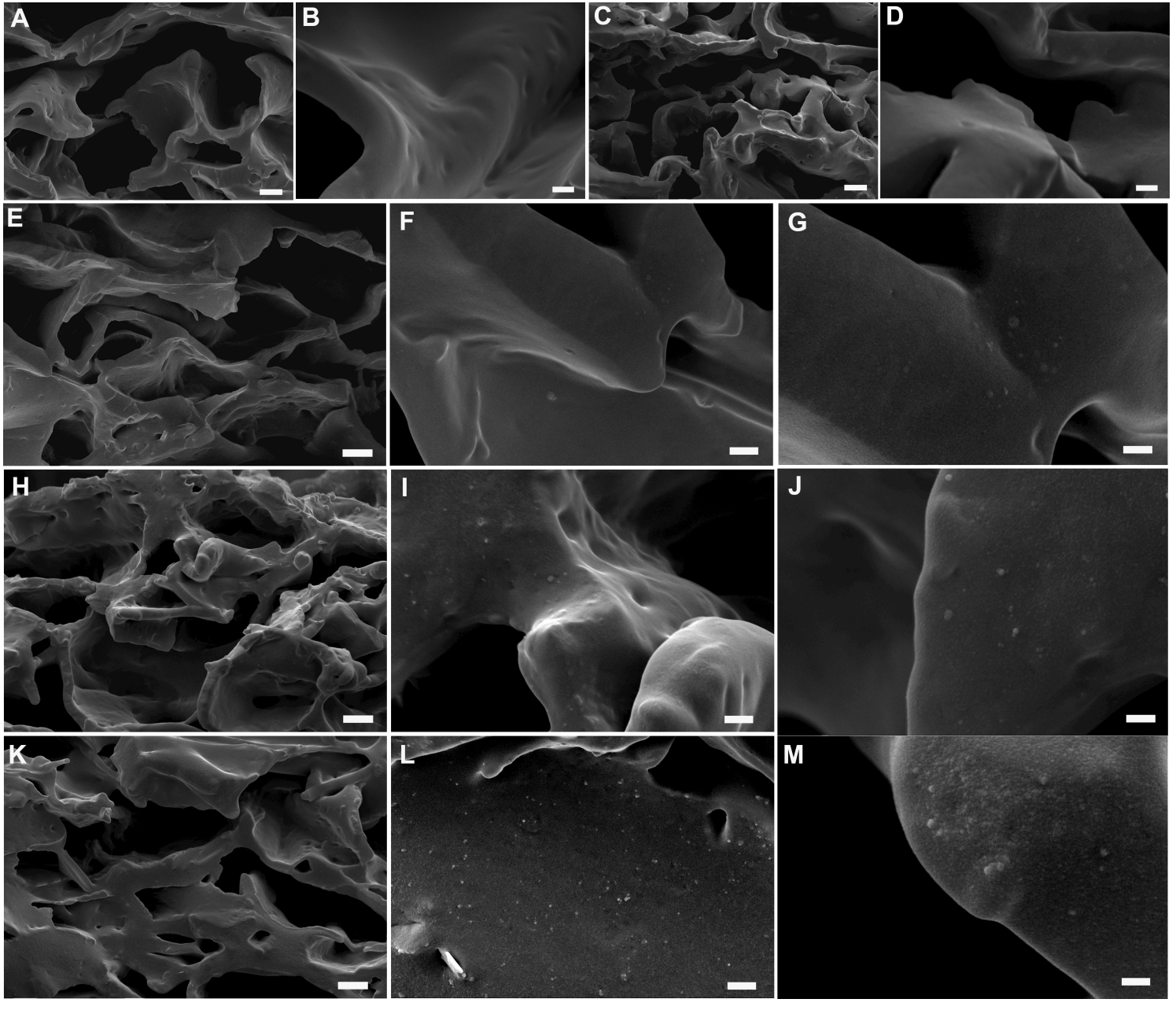
A
B
C
D
E
F
G
H
I
J
K
L
M

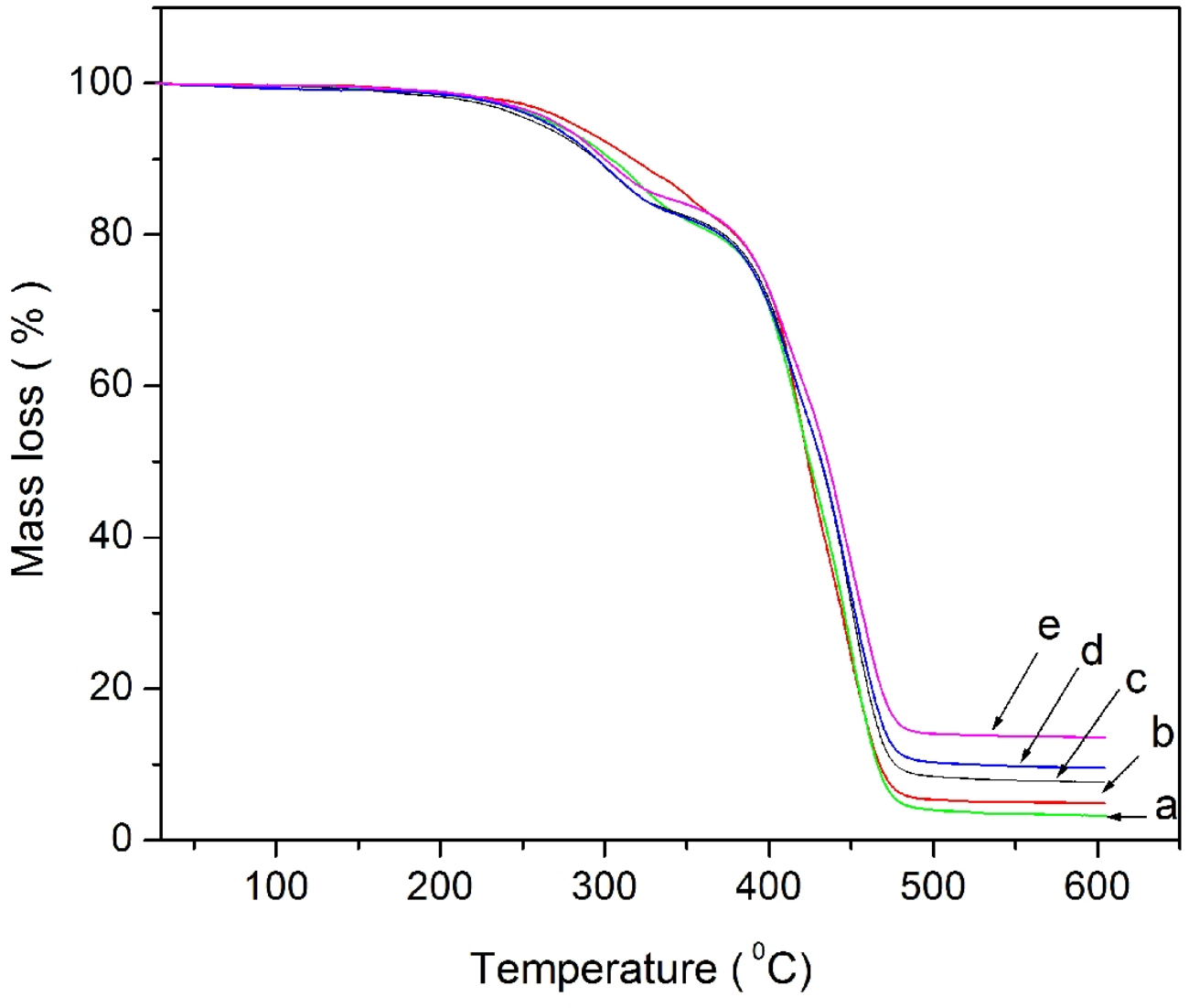
Mass loss (%)
100
80
60
40
20
0
100
200
300
400
500
600
Temperature (°C)
e
d
c
b
a

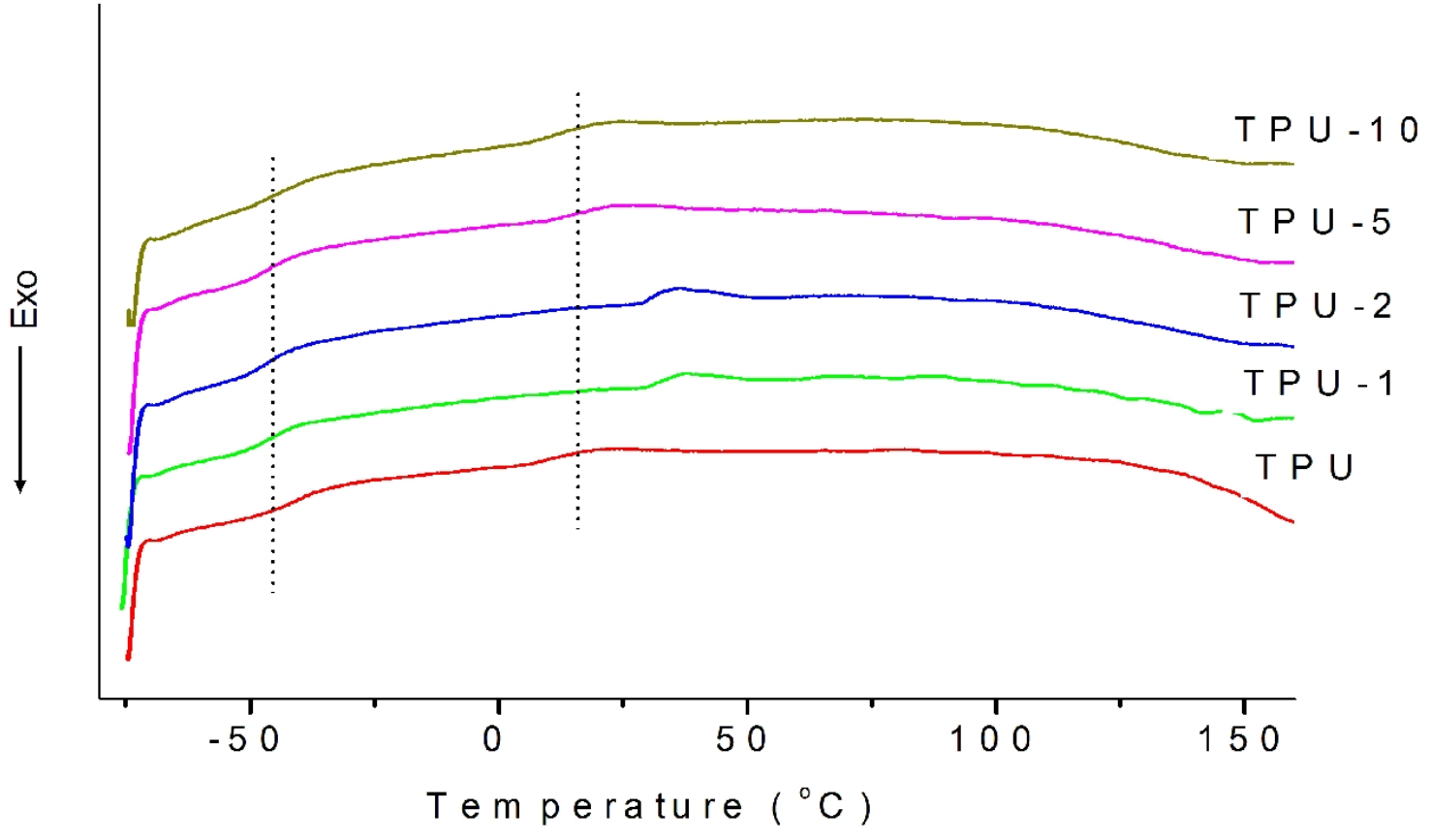
TPU-10
TPU-5
TPU-2
TPU-1
TPU
Exo
-50
0
50
100
150
Temperature (°C)

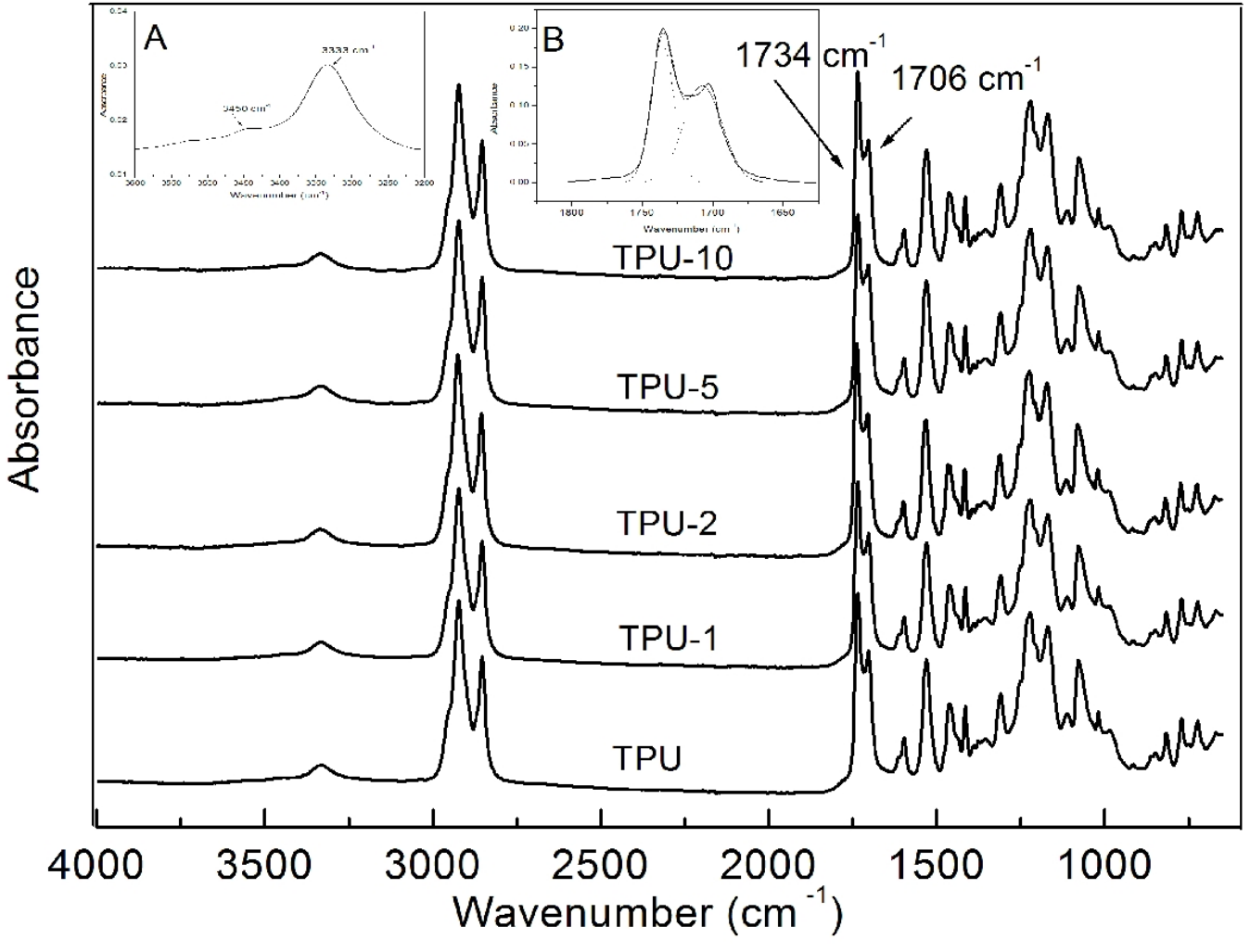
A
B
3333 cm-1
3450 cm-1
1734 cm-1
1706 cm-1
TPU-10
TPU-5
TPU-2
TPU-1
TPU
Absorbance
4000
3500
3000
2500
2000
1500
1000
Wavenumber (cm-1)

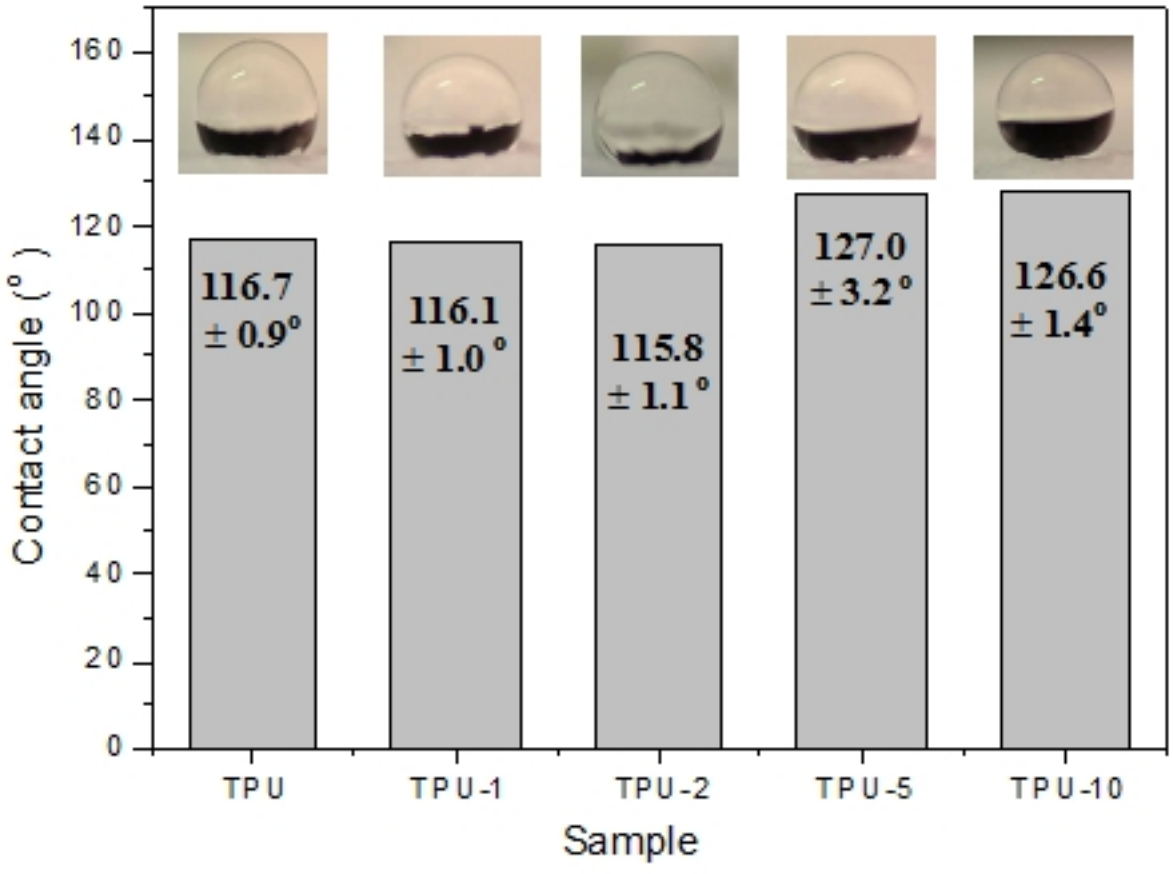
Contact angle (°)
160
140
120
100
80
60
40
20
0
116.7
± 0.9°
116.1
± 1.0 °
115.8
± 1.1 °
127.0
± 3.2°
126.6
± 1.4°
TPU
TPU-1
TPU-2
TPU-5
TPU-10
Sample

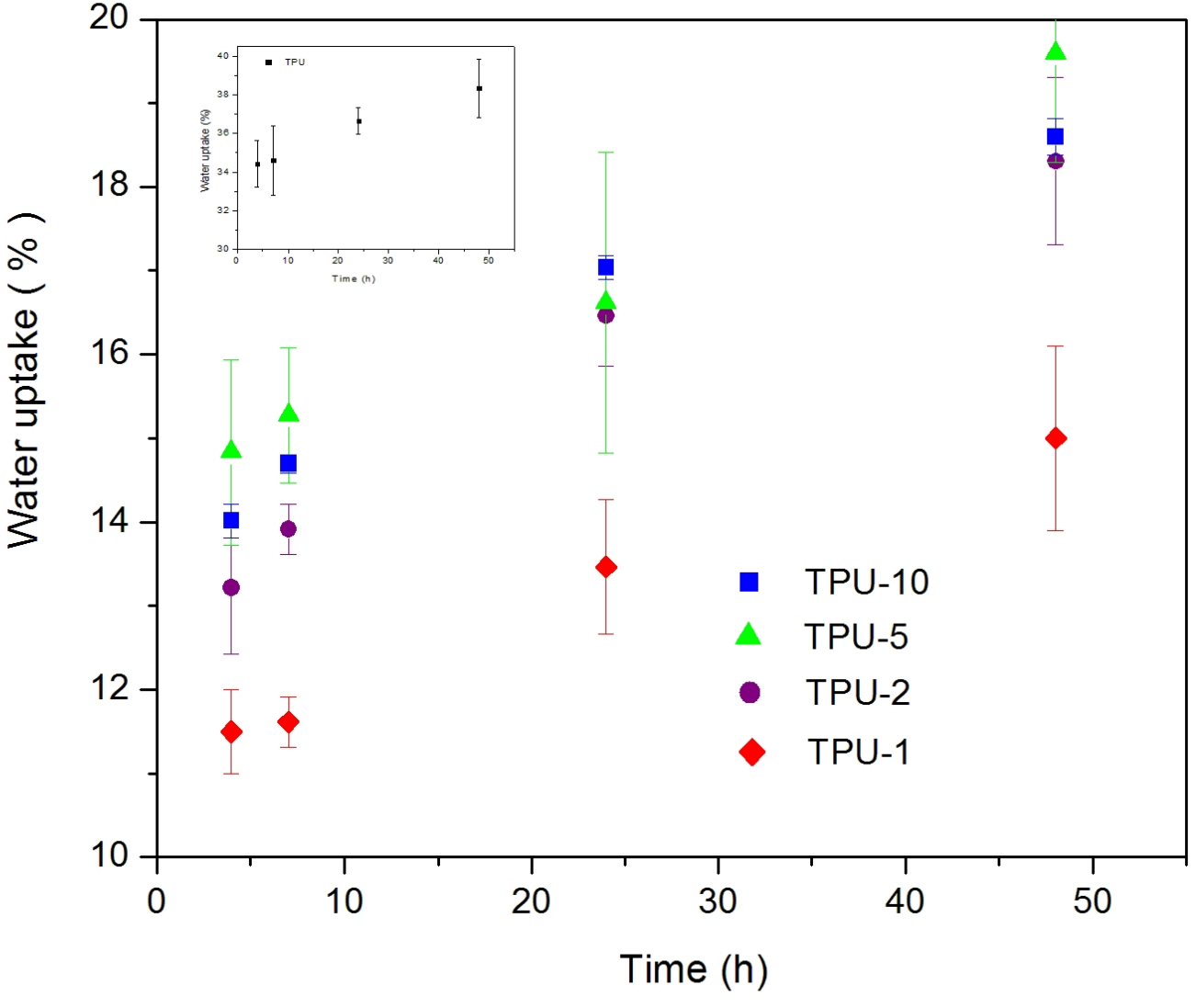
Water uptake (%)
Time (h)
TPU-10
TPU-5
TPU-2
TPU-1
TPU
Water uptake (%)
Time (h)

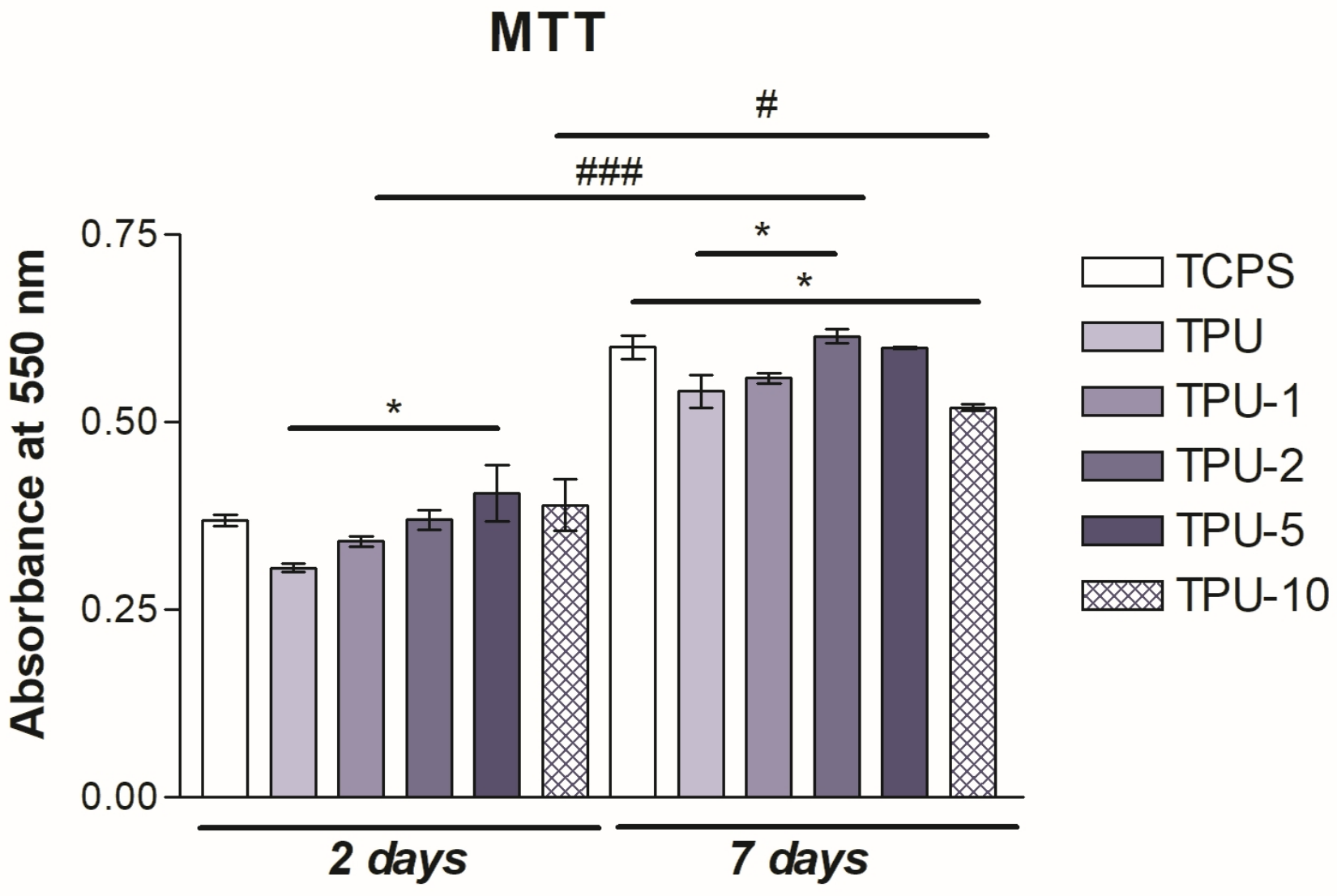
MTT
#
###
*
*
*
Absorbance at 550 nm
0.75
0.50
0.25
0.00
2 days
7 days
TCPS
TPU
TPU-1
TPU-2
TPU-5
TPU-10

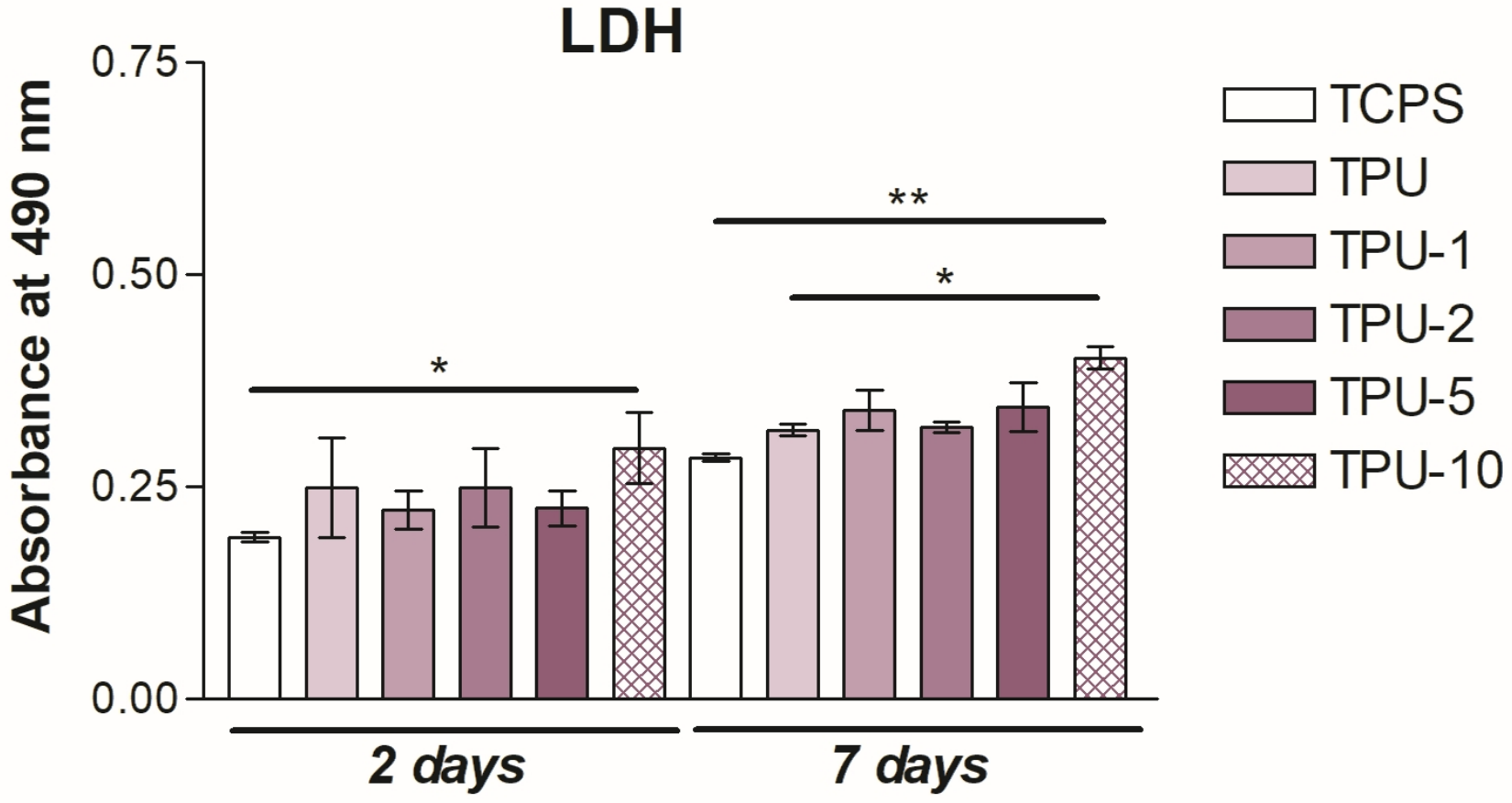
LDH
Absorbance at 490 nm
0.75
0.50
0.25
0.00
*
**
*
2 days
7 days
TCPS
TPU
TPU-1
TPU-2
TPU-5
TPU-10

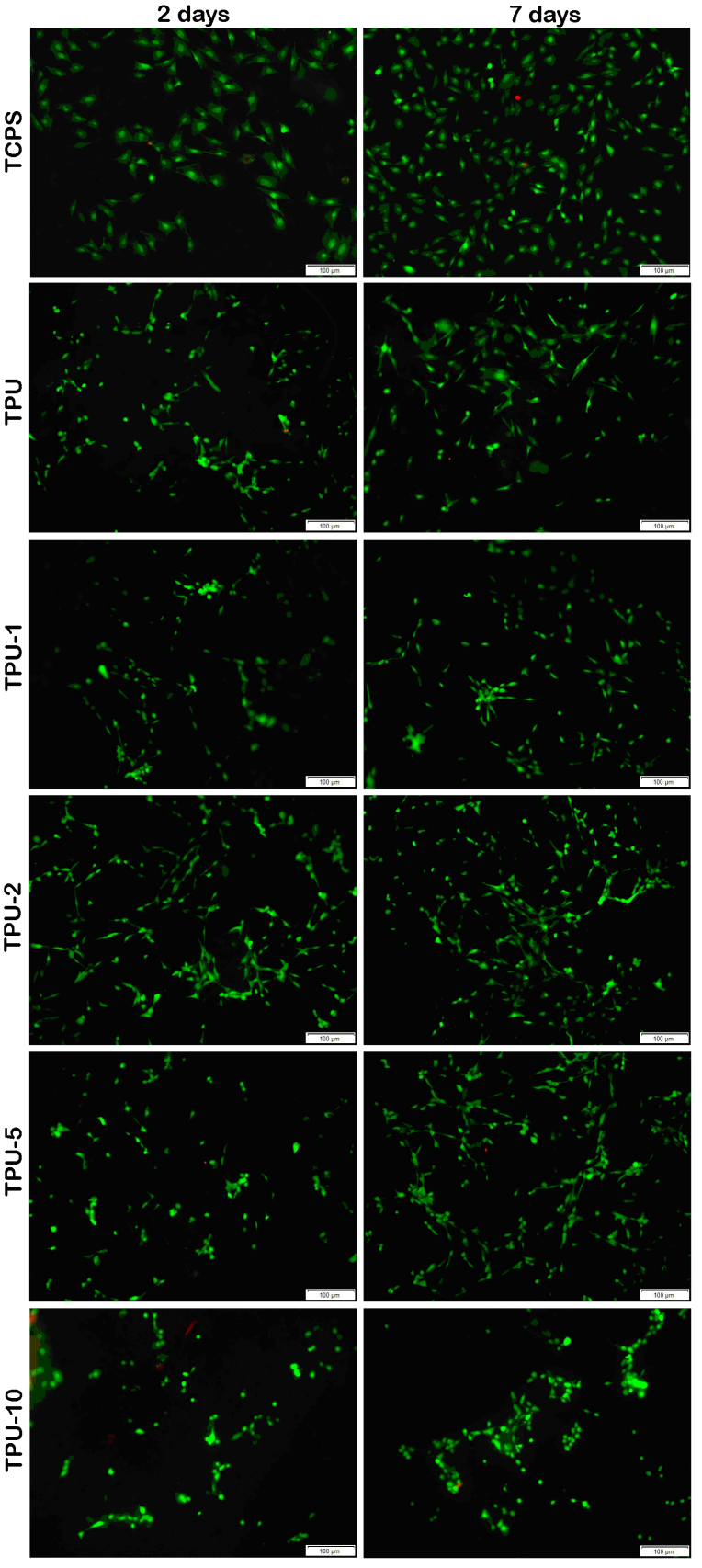
2 days
7 days
TCPS
TPU
TPU-1
TPU-2
TPU-5
TPU-10

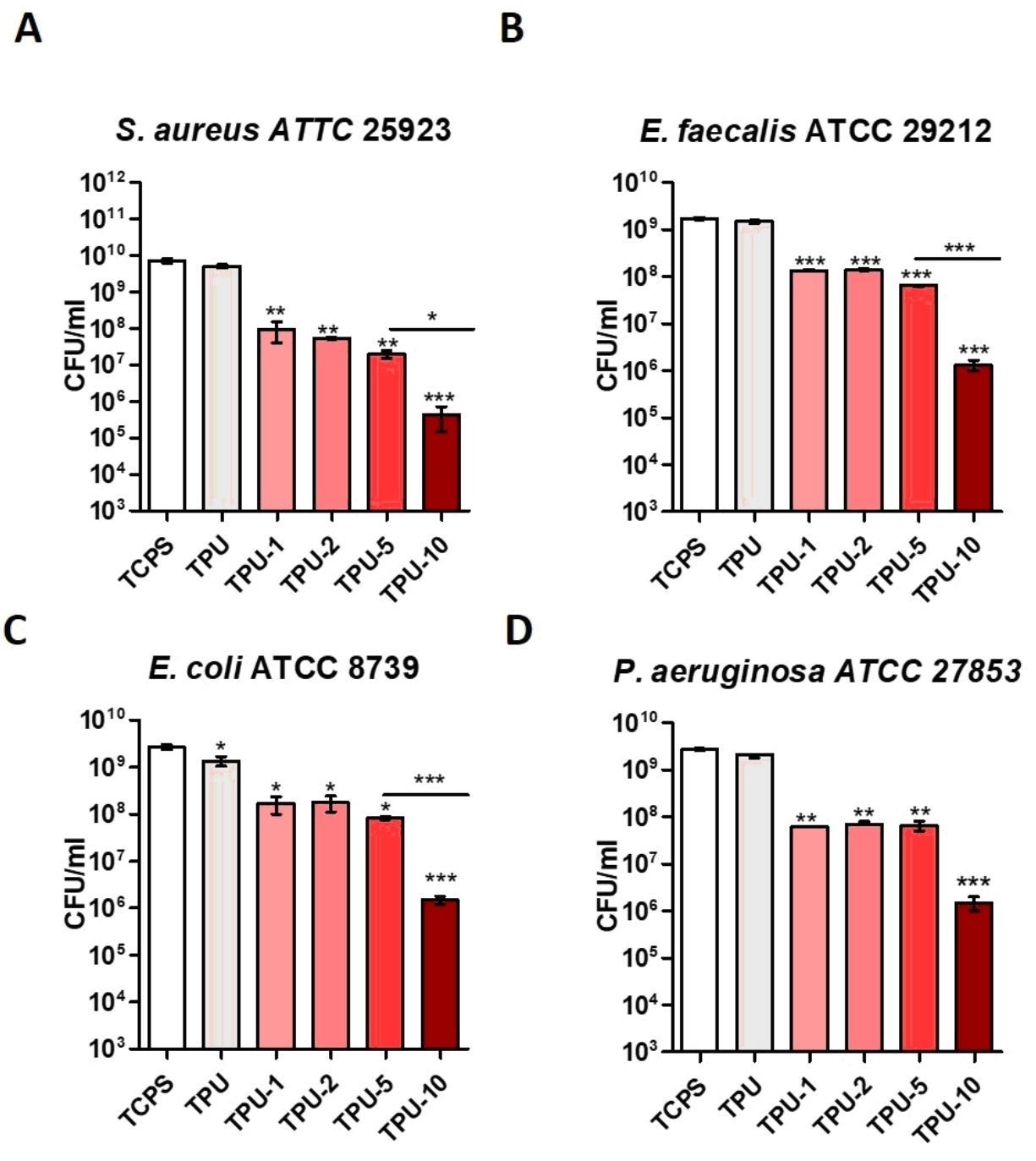
A
S. aureus ATTC 25923
CFU/ml
TCPS
TPU
TPU-1
TPU-2
TPU-5
TPU-10
B
E. faecalis ATCC 29212
C
E. coli ATCC 8739
D
P. aeruginosa ATCC 27853

Table 1
Sample labeling and composition of TPU/ZnO foams

Sample	TPU/ZnO w/w (%)
TPU	100/0
TPU-1	99/1
TPU-2	98/2
TPU-5	95/5
TPU-10	90/10

Table 2
Thermal properties of TPU/ZnO nanocomposite foams obtained from TGA and DSC measurements

	TGA data			DSC data[a]			
Sample	$T_{onset\ 1}$ (°C)	$T_{onset\ 2}$ (°C)	m_{res}[b] (%)	T_{g1} (°C)	ΔC_{p1} (J $g^{-1}K^{-1}$)	T_{g2} (°C)	ΔC_{p2} (J $g^{-1}K^{-1}$)
TPU	265	394	4.8	-44.6	0.19	11.3	0.16
TPU-1	261	404	6.0	-46.4	0.29	33.8	0.25
TPU-2	259	409	6.9	-45.9	0.23	31.1	0.19
TPU-5	257	401	9.9	-46.1	0.18	17.9	0.18
TPU-10	256	400	14.5	-44.8	0.15	14.9	0.29

[a] DSC first scan
[b] at 600°C

Table 3
Deconvoluted peaks and HBI for TPU and TPU/ZnO nanocomposite foams

Peaks (cm^{-1})			
	1706	1734	
Sample	Integrated areas[a]		HBI[b]
TPU	3.65	3.54	1.03
TPU-1	4.21	3.52	1.19
TPU-1	4.21	3.56	1.18
TPU-5	4.46	3.26	1.36
TPU-10	4.11	3.60	1.14

[a] Integrated area of deconvoluted peaks
[b] Hydrogen bonding index

Table 4
Water vapour transmission rate for TPU and TPU/ZnO nanocomposite foams

Sample	WVTR[a] ($mg/cm^2 \cdot h$)
TPU	8.9 ± 0.09
TPU-1	8.3 ± 0.12
TPU-2	8.0 ± 0.06
TPU-5	8.2 ± 0.11
TPU-10	8.1 ± 0.03

[a] WVTR was determined as a slope of the function weight changes versus time

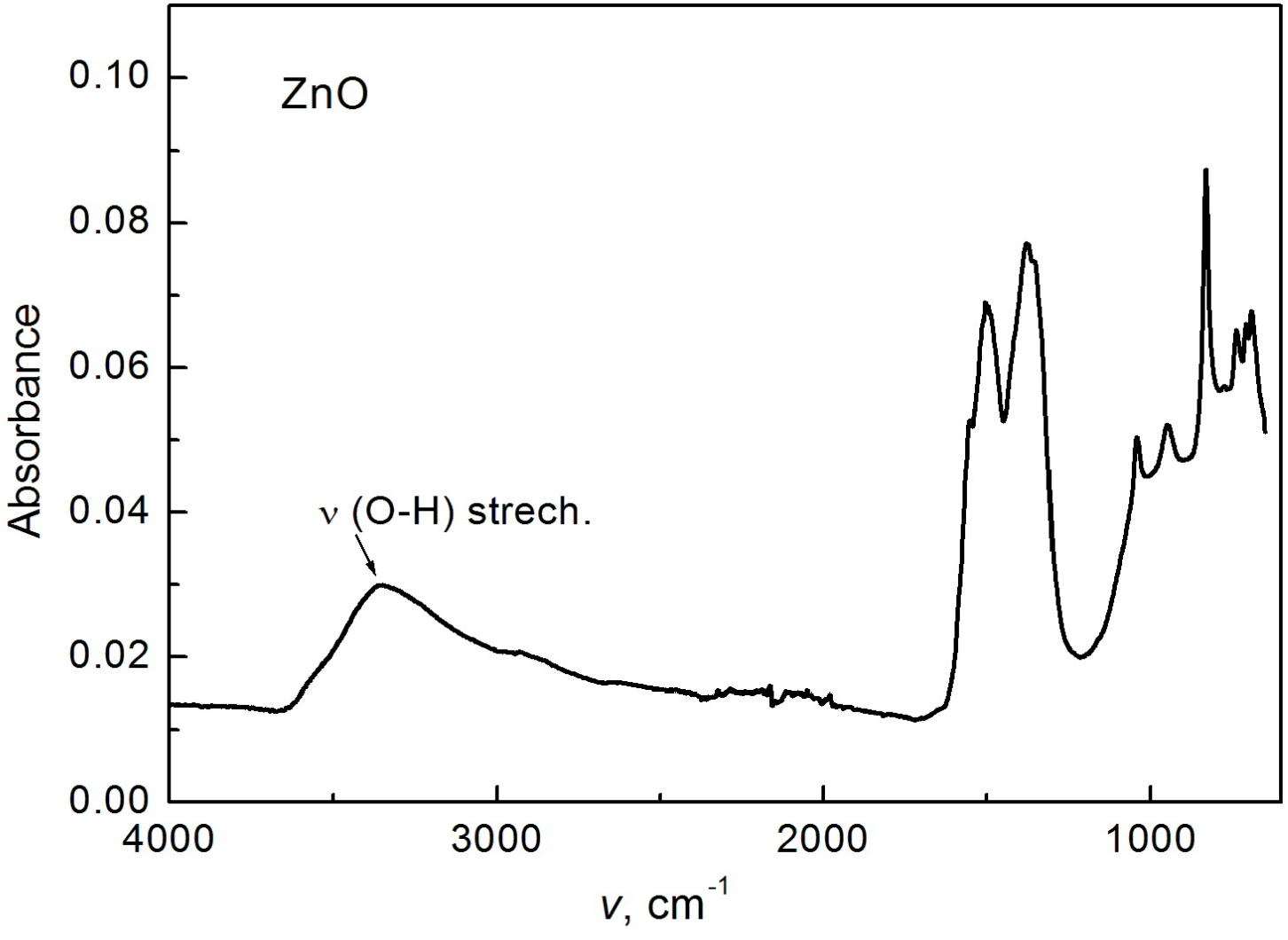
ZnO
ν (O-H) strech.
Absorbance
0.00
0.02
0.04
0.06
0.08
0.10
4000
3000
2000
1000
ν, cm-1

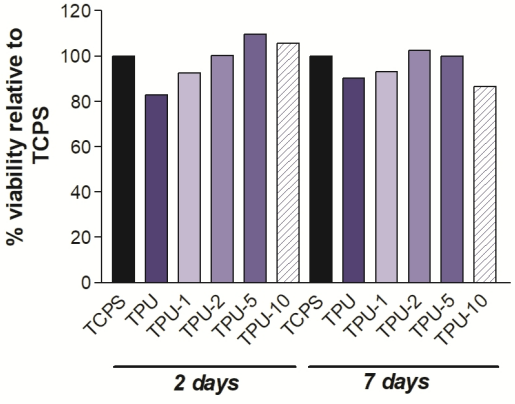
% viability relative to TCPS
120
100
80
60
40
20
0
TCPS
TPU
TPU-1
TPU-2
TPU-5
TPU-10
2 days
7 days

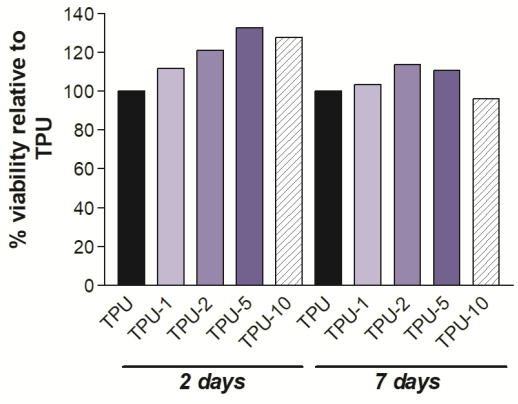
% viability relative to TPU
140
120
100
80
60
40
20
0
TPU
TPU-1
TPU-2
TPU-5
TPU-10
2 days
7 days

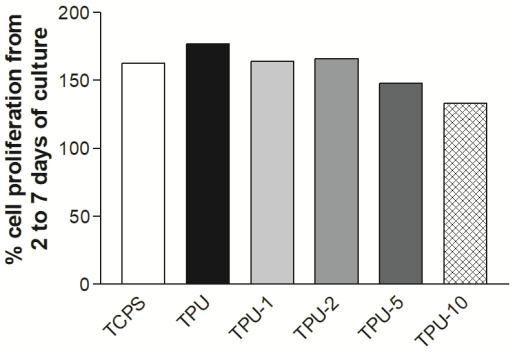
% cell proliferation from 2 to 7 days of culture
200
150
100
50
0
TCPS
TPU
TPU-1
TPU-2
TPU-5
TPU-10

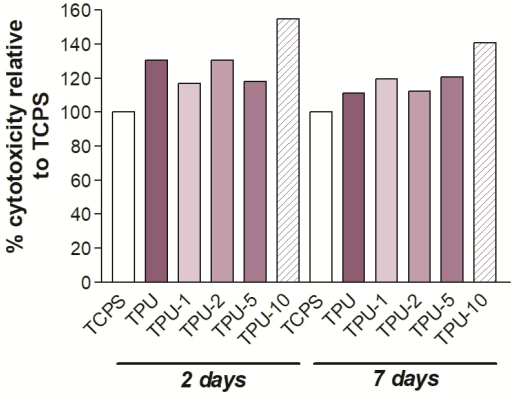
% cytotoxicity relative to TCPS
160
140
120
100
80
60
40
20
0
TCPS
TPU
TPU-1
TPU-2
TPU-5
TPU-10
2 days
7 days

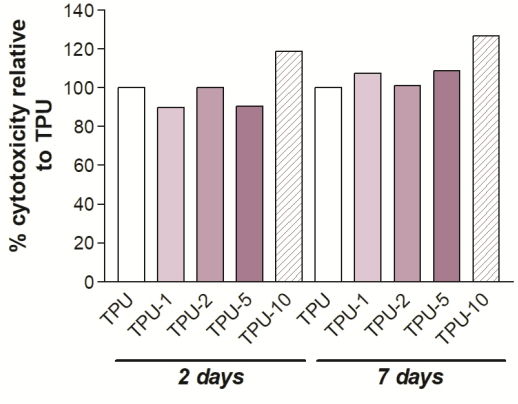
% cytotoxicity relative to TPU
140
120
100
80
60
40
20
0
TPU
TPU-1
TPU-2
TPU-5
TPU-10
2 days
7 days

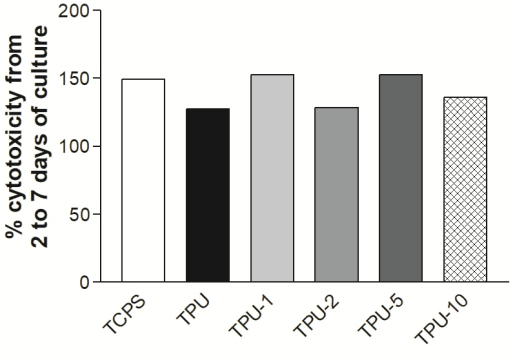
% cytotoxicity from 2 to 7 days of culture
200
150
100
50
0
TCPS
TPU
TPU-1
TPU-2
TPU-5
TPU-10